Correlation and Taylor scale variability in the interplanetary magnetic field fluctuations as a function of solar wind speed

James M. Weygand,[1] W. H. Matthaeus,[2] S. Dasso,[3] and M. G. Kivelson[4,5]

Received 4 March 2011; revised 9 May 2011; accepted 23 May 2011; published 20 August 2011.

[1] Simultaneous multiple point measurements of the magnetic field from 11 spacecraft are employed to determine the correlation scale and the magnetic Taylor microscale of the solar wind as functions of the mean magnetic field direction and solar wind speed. We find that the Taylor scale is independent of direction relative to the mean magnetic field in both the slow (<450 km/s) and the fast (>600 km/s) solar wind, but the Taylor scale is longer along the mean magnetic field direction in the intermediate (600 km/s ≥ speed ≥ 450 km/s) solar wind. The correlation scale, on the other hand, varies with angle from the mean magnetic field direction. In the slow solar wind the ratio of the parallel correlation scale to the perpendicular correlation scale is 2.55 ± 0.76, decreases to 2.15 ± 0.18 in the intermediate solar wind, and becomes 0.71 ± 0.29 in the fast solar wind. Thus, solar wind turbulence is anisotropic, dominated by quasi two-dimensional turbulence in both the slow and intermediate solar wind, and by slab type turbulence in the fast solar wind. The correlation and Taylor scales may be used to estimate effective magnetic Reynolds numbers separately for each angular channel. To within the uncertainty, no dependence on the solid angle relative to the mean magnetic field could be identified for the Reynolds number. These results may be useful in magnetohydrodynamic modeling of the solar wind and can contribute to our understanding of solar and galactic cosmic ray diffusion in the heliosphere.

Citation: Weygand, J. M., W. H. Matthaeus, S. Dasso, and M. G. Kivelson (2011), Correlation and Taylor scale variability in the interplanetary magnetic field fluctuations as a function of solar wind speed, *J. Geophys. Res.*, *116*, A08102, doi:10.1029/2011JA016621.

1. Introduction

[2] In the cascade picture of broadband turbulence, energy input occurs mainly at large scales but is transferred across scales by nonlinear processes, eventually reaching small scales where dissipation mechanisms of kinetic origin limit the transfer, dissipate the fluid motions, and convert kinetic energy into heat. This general picture is expected in hydrodynamics and in fluid plasma models such as magnetohydrodynamics (MHD) when the associated Reynolds number and magnetic Reynolds number are large compared to unity, implying that nonlinear couplings are much stronger than the dissipation processes at large scales and that structures having a wide range of spatial scales are involved in the dynamics. In the MHD limit, flows and field perturbations are clearly coupled, implying that their properties are closely related. Spectra of fluctuations of the magnetic field (as well as other quantities such as velocity and density) are found to be broadbanded in the solar wind. Many studies of magnetic field and solar wind flow turbulence analyze the cascade process through spectral analysis [*Goldstein et al.*, 1994, 1995] or through analysis of structure functions [*Burlaga and Klein*, 1986; *Burlaga*, 1991a, 1991b, 1991c; *Tu and Marsch*, 1995] at various orders. Spectral analysis emphasizes the self-similar range of scale properties that give rise to descriptions such as the famous power law of Kolmogorov theory [*Kolmogorov*, 1941] and its variants [*Kraichnan*, 1965].

[3] The self-similar range is typically defined as extending from an energy-containing scale (large scale) down to a Kolmogorov dissipation scale. Thus the two most studied length scales are those that define the long wavelength and short wavelength ends of the power law inertial spectral range. The energy-containing scale is typically of the same order as the correlation scale λ_{CS}, which can be measured using classical methods based on the assumption of Taylor frozen-in flow and can be associated with the first bend-over point in a power spectrum of the turbulent fluctuations. This bend–over point or the long wavelength end of the inertial range starts at scale smaller than both the energy containing scale and correlation scale. The dissipation scale L_{diss} is the scale at which the turbulent cascade is critically damped and significant energy is

[1]Institute of Geophysics and Planetary Physics, University of California, Los Angeles, California, USA.
[2]Bartol Research Institute, Department of Physics and Astronomy, University of Delaware, Newark, Delaware, USA.
[3]Instituto de Astronomía y Física del Espacio, Departmento de Física, Facultad de Ciencias Exactas y Naturales, Universidad de Buenos Aires, Buenos Aires City, Argentina.
[4]Department of Atmospheric, Oceanic and Space Sciences, University of Michigan, Ann Arbor, Michigan, USA.
[5]Department of Earth and Space Sciences, University of California, Los Angeles, California, USA.

0148-0227/11/2011JA016621

deposited into heat. This scale can be associated with the second bend-over point in a power spectrum.

[4] Another fundamental turbulence scale, the magnetic Taylor microscale, is approximately the wave number (k) within power spectra at which damping of the turbulent eddies in the cascade begins to become more important and corresponds to smaller k (larger wavelengths) than the dissipation scale. In hydrodynamics the Taylor microscale may be interpreted as the length at which the eddy viscous dissipation time $(k^2\nu)^{-1}$, where ν is the viscosity, becomes equal to the global eddy turnover time λ_{CS}/u where u is the bulk speed. With the hydrodynamics definition of the Taylor microscale and the large scale Reynolds number given as $R = u\,\lambda_{CS}/\nu$, the Taylor and correlation scales are related by [*Batchelor*, 1970]

$$R_{eff} = \left(\frac{\lambda_{CS}}{\lambda_T}\right)^2. \quad (1)$$

The effective Reynolds number, correlation scale, and Taylor scale and their possible anisotropy are important parameters for understanding the nature of turbulence in a plasma and for determining whether the parameters of numerical MHD models match those of the space plasmas that they model. In this study we focus on variation of the correlation scale with direction relative to the magnetic field for three different ranges of solar wind speed. We use the derived values to calculate the effective magnetic Reynolds number and to investigate its dependence on flow speed and direction relative to the magnetic field.

[5] In the related fields of plasma physics, magnetohydrodynamics and space plasmas, turbulence has been analyzed by procedures analogous to those used in hydrodynamics. If the mean velocity of the flow relative to a spacecraft is supersonic and super-Alfvénic, the correlation scale is often evaluated from single point measurements by assuming the fluctuations are frozen-into the flow. This assumption introduces errors related to the temporal evolution of the medium, which may result from the presence of dispersive waves with possibly high phase velocities or other time variations. Correlation scales can also be computed using the two-point, or two spacecraft method outlined by *Matthaeus et al.* [2005] and avoid errors introduced by temporal evolution of the medium.

[6] Although the Taylor scale has been evaluated in hydrodynamic systems, the analog of the Taylor microscale in space plasmas has been almost completely ignored prior to *Matthaeus et al.* [2005], mainly because of instrumental limitations including cadence and instrumental uncertainty. In recent years with the increased availability of high time resolution magnetic field measurements, *Matthaeus et al.* [2005], *Weygand et al.* [2007], and *Weygand et al.* [2009] have been able to estimate the Taylor microscale, which they have determined to be approximately the radius of curvature of the two-point magnetic field correlation function in the limit of zero separation. See those studies for more details on the procedure for determining the Taylor scale.

[7] Turbulent magnetic field fluctuations observed in the solar wind are thought to be the driven by two different sources. One source of turbulence, which consists of Alfvén waves where the fluctuation wave vectors are approximately aligned with the mean magnetic field, is thought to originate in part in regions of the solar atmosphere where it is imposed by coronal dynamical processes. The other source of turbulent magnetic field fluctuations, which consists of wave vectors and magnetic field fluctuations approximately perpendicular to the mean magnetic field, may be driven by stream interactions, including compressions and shears in the solar wind [*Roberts et al.*, 1987]. These drivers may also be responsible for the heating that underlies the observed highly nonadiabatic temperature profile that extends from inside 1 AU to beyond 60 AU as observed by Voyager and Pioneer [*Gazis et al.*, 1994; *Richardson et al.*, 1995; *Williams et al.*, 1995; *Smith et al.*, 2001]. However, the temperature profile may also be influenced by adiabatic cooling, dissipation of waves, and the transfer of energy from pickup ions to thermal protons [*Richardson and Smith*, 2003].

[8] Anisotropy of solar wind magnetic field turbulence, which refers to the variation of the turbulent properties with angle relative to the mean magnetic field direction, affects the propagation and acceleration of cosmic rays [*Duffy and Blundell*, 2005] and the heating of the interplanetary plasma [*Velli*, 2003]. Anisotropic magnetic field fluctuations have been interpreted using both the slab model and the "two-dimensional" model. In the slab model, the wave vectors consist of Alfvén waves whose wave vectors are aligned with the mean magnetic field. The correlation function for this model has the shortest scales parallel to the mean magnetic field and the longest scale in the perpendicular direction [*Dasso et al.*, 2005; *Osman and Horbury*, 2007]. The slab model does not, however, allow for wave-wave coupling in the case of incompressible MHD and thus cannot produce a turbulent Kolmogorov-like cascade like or Iroshnikov-Kraichnan like cascade [*Oughton and Matthaeus*, 2005]. In the two-dimensional model, which does allow for mode coupling, the excited wave vectors and magnetic field fluctuations lie in the plane perpendicular to the mean magnetic field; the correlation function has the shortest scales in the perpendicular direction and longer scales in the parallel direction [*Dasso et al.*, 2005; *Osman and Horbury*, 2007]. A superposition of slab and two-dimensional fluctuations forms a convenient parameterized model for anisotropy that has been employed for convenience in a variety of applications [e.g., *Bieber et al.*, 1994] including cosmic ray scattering [*Ruffolo et al.*, 2004].

[9] In this study, anisotropy is taken to imply a dependence of the fundamental scale lengths on the angle between the turbulent fluctuations and the direction of the mean magnetic field. To characterize the anisotropy without adopting the frozen-in flow approximation, simultaneous two point measurements of the turbulent fluctuations at a variety of angles relative to the mean magnetic field direction are required. Previous analyses of anisotropy typically have used data from single spacecraft and assumed frozen-in fields. For example, in one early study, *Matthaeus et al.* [1990] employed magnetic field fluctuations measured by ISEE 3 in the solar wind, and found an anisotropic correlation function with a "Maltese cross" shape. They interpreted this shape using as an approximate simplified representation a superposition of slab and two-dimensional fluctuations. *Bieber et al.* [1996] examined the ratio of the perpendicular and quasi-parallel spectra, along with the dependence of the total power spectrum on the angle between the mean magnetic field and the solar wind flow direction, to measure the relative amplitudes

of the slab and two-dimensional power. They found that about 85% of the energy was in the two-dimensional component. *Dasso et al.* [2005], using autocorrelation measurements from a single spacecraft, took the work of *Matthaeus et al.* [1990] one step further by subdividing the solar wind magnetic field and plasma flow data into fast (>500 km/s) and slow (<400 km/s) solar wind intervals. In both the magnetic field and flow data, they found that quasi two-dimensional fluctuations dominate in the slow solar wind and slab fluctuations are more prominent in the fast solar wind. In a recent solar wind study, *Osman and Horbury* [2007] used multi-spacecraft time-lagged two-point correlation measurements obtained by the Cluster mission to construct a spatial autocorrelation function. For one solar wind interval with an average speed of 330 km s^{-1}, they demonstrated that the solar wind fluctuations are anisotropic by showing that the ratio of the correlation length along the magnetic field to the perpendicular correlation length is 1.79 ± 0.36. From numerical simulations of incompressible, three dimensional, MHD turbulence, *Milano et al.* [2001] obtained results similar to the observations of *Osman and Horbury* [2007], demonstrating that the correlation scale along the locally averaged magnetic field direction is longer than along the direction perpendicular to the local mean magnetic field.

[10] The goal of this study is to obtain the correlation and Taylor scales as functions of the angle relative to the mean magnetic field in the slow, intermediate, and fast solar wind. In previous papers we presented preliminary results on the correlation scale and the Taylor scale in solar wind turbulence using simultaneous two point measurements acquired by pairs of interplanetary spacecraft [*Matthaeus et al.*, 2005; *Weygand et al.*, 2007, 2009] but not distinguishing among different solar wind speed ranges. In the Matthaeus et al. study, the correlation scale was determined from a robust fit of an exponential function to the data. In the *Weygand et al.* [2007] study, the Taylor scale was determined from a new method based on the Richardson extrapolation technique. *Weygand et al.* [2009] also accumulated two-spacecraft samples in sufficient numbers to resolve the correlations into angular bins relative to the locally computed mean magnetic field and demonstrated a variation of the correlation scale with the angle relative to the mean magnetic field direction. The approach here is similar; however we have enough data to bin the cross correlations into three different solar wind speed ranges. This makes possible a two-spacecraft study of anisotropy of the correlation scale and the Taylor scale as a function of the solar wind speed.

[11] In the following sections we refer to the above mentioned references for methodological details. We use our augmented database of two spacecraft correlation data to determine the Taylor scale (λ_T) and the correlation scale (λ_{CS}) in the interplanetary plasma. Each type of measurement is resolved in angular channels to characterize properties of anisotropy relative to the mean magnetic field. We will also derive quantitative estimates of the effective magnetic Reynolds number. Finally, we compare our results with previously published estimates based on single and multi spacecraft observations of the associated scales.

2. Instrumentation

[12] The magnetic field measurements were obtained from Cluster, ACE, Geotail, IMP 8, Interball, THEMIS, and Wind. This large number of spacecraft provides effectively simultaneous two-point plasma and field measurements at a large range of spatial separations, enabling us to measure spatial correlations as a function of separation directly instead of inferring them by interpreting temporal fluctuations as frozen into a flowing plasma [*Taylor*, 1938].

[13] The Cluster mission, supported jointly by the European Space Agency (ESA) and National Aeronautics and Space Administration (NASA), consists of four identical spacecraft with a perigee of 4 R_E, an apogee of 19.6 R_E, and a spin period of about 4 s. These four spacecraft provide the first three-dimensional measurements of large- and small-scale phenomena in the near-Earth environment [*Escoubet et al.*, 1997]. Each Cluster spacecraft carries 11 instruments. This study uses data from the magnetometer (FGM) [*Balogh et al.*, 1997] and the ion spectrometer (CIS) [*Rème et al.*, 1997]. The Cluster apogee precesses around the Earth annually. From 2001 to 2007, between January and April the Cluster spacecraft apogees were intermittently in the solar wind. At apogee in the summer seasons, the spacecraft were located at the vertices of nearly regular tetrahedrons. The scales of the tetrahedral differed from one season to the next, covering a range of distances pertinent to turbulence studies. In the solar wind seasons of 2001 and 2004, the tetrahedron's scale was about 1000 km, which is close to the short wavelength limit of the inertial range. During the 2002 season the scale was 5000 km. From January and April 2003, Cluster obtained another series of solar wind intervals at an interspacecraft spacing of about 100 km (i.e., on the order of dissipation range). In the solar wind seasons of 2005 and 2006 the tetrahedral formation was not used; instead two pairs of spacecraft were separated by about 10,000 km and the separation within a pair was 1000 km. In 2007 two of the spacecraft were within a few 100 km of one another and the other two had a separation of about 10,000 km from each other and the pair.

[14] Each Cluster spacecraft carries a boom-mounted triaxial fluxgate magnetometer [*Balogh et al.*, 1997]. Magnetic field vectors routinely are available at 22 Hz resolution (nominal mode). Both preflight and in-flight calibrations of the two magnetometers have produced carefully calibrated (and intercalibrated) magnetic field data. The relative uncertainty in the data after calibration is at most 0.1 nT, an estimate determined by examining the drift in the offset after calibration (K. K. Khurana and H. Schwarzl, private communication, 2004). The digital resolution of the magnetometer is on the order of 8 pT [*Balogh et al.*, 1997].

[15] Data from the CIS instrument [*Rème et al.*, 1997], along with the magnetic field data, are essential in identifying periods when Cluster enters the solar wind. CIS provides bulk plasma parameters such as density, velocity, the pressure tensor, and heat flux. The uncertainties in most of these quantities are not significant for this study. Although plasma data not are available from all four spacecraft, intervals in the solar wind can be established from single spacecraft measurements because the spacecraft are close to one another.

[16] Magnetic field and plasma data from 2 of the 5 THEMIS spacecraft, which were launched in February 2007, are also used. Only THEMIS B and C entered the solar wind. From approximately mid June to mid October their apogees align on the dayside of the magnetosphere and provide

spacecraft separations on the order of 10 R_E. In mid 2009 the orbits of the THEMIS B and C spacecraft were altered in order to insert them into orbit around the moon for future lunar studies. This change in the orbits provided data for additional spacecraft separations ranging from 10 to 30 R_E.

[17] Each THEMIS spacecraft carries a boom-mounted triaxial fluxgate magnetometer (FGM) [*Auster et al.*, 2008]. Magnetic field vectors routinely are available at 64 Hz resolution (nominal mode). Both preflight and in-flight calibrations of the two magnetometers have been performed. The relative uncertainty in the data after calibration is about 0.1 nT, an estimate determined by examining the drift in the offset after calibration (H. U. Auster and V. Angelopoulos, personal communication, 2010). The digital resolution of the magnetometer is on the order of 0.01 nT [*Auster et al.*, 2008].

[18] As for Cluster, particle data, this time from the THEMIS ESA instrument [*McFadden et al.*, 2008], along with the magnetic field data, are essential in identifying periods when THEMIS enters the solar wind. ESA provides bulk plasma parameters such as density, velocity, the pressure tensor, and heat flux. The uncertainties in most of these plasma parameters are not significant for this study as their data are used only to identify intervals in the solar wind is important.

[19] From the ACE, Geotail, IMP 8, Interball, and Wind spacecraft we use data from triaxial fluxgate magnetometers [*Smith et al.*, 1998; *Kokubun et al.*, 1994; *Nozdrachev et al.*, 1995; *Lepping et al.*, 1995] to obtain the local IMF direction and magnitude at temporal resolutions ranging from 3 s to 16 s. Data from the ACE Solar Wind Electron Proton Alpha Monitor (SWEPAM) [*McComas et al.*, 1998], the Geotail Comprehensive Plasma Instrument (CPI) and Low Energy Particle (LEP) experiment [*Frank et al.*, 1994; *Mukai et al.*, 1994], IMP 8 Plasma Faraday Cup [*Lazarus and Paularena*, 1998], and Wind 3-D plasma and energetic particle instrument (3DP) [*Lin et al.*, 1995] provide the solar wind speed and density at temporal resolutions ranging from 3 s to 64 s.

3. Procedure and Observations

[20] The first step in this study was to select intervals that could be confidently identified as being within the solar wind. The Cluster and THEMIS solar wind data intervals are selected visually from plotted data by excluding data at or within the bow shock. The solar wind is identified from the plasma density, which was of the order of several particles per cm^{-3}, and the solar wind speed, which was greater than or equal to 250 km s^{-1}. Neither the magnetic field nor the plasma densities are limited to a specific range. The choice of 250 km s^{-1} as a cutoff velocity, although arbitrary, excludes magnetosheath data. We also limit our observations to local times within a few hours of noon to avoid the high speed flows that occur within the magnetosheath on the flanks of the magnetosphere. We do not use solar wind data with sharp rotations in the B_x and B_y GSE components in order to exclude sector boundary crossings. We remove solar wind shocks and gradients within the flow, density, and total magnetic field that occur over a time range of a few minutes. The Cluster and THEMIS spacecraft remain relatively close together (<25 R_E) and are used to characterize fluctuations over short distances. For analysis of these short distance separations, we include data from intervals of 1 h or longer. The Cluster and THEMIS orbits remained in relatively close proximity to the bow shock, even when in the solar wind. Inevitably foreshock waves are present in some of the selected intervals. To minimize the contribution of such waves to our analysis, the solar wind magnetic field measurements are averaged to 30 s resolution, which is approximately the longest period for ion foreshock waves. In order to test whether the averaging does effectively eliminate foreshock-related effects, we analyzed a subset of solar wind intervals when no foreshock waves or shocklets were present and found that the results were similar to those in the full data set.

[21] Data from the ACE, Geotail, IMP 8, Interball, and Wind spacecraft yield cross correlations at larger separations than those of Cluster and THEMIS. In order to obtain meaningful cross correlation coefficients at larger separations, we require longer continuous intervals for analysis. Therefore, for the larger separations, we do not accept intervals with less than 12 h of continuous data at 1 min resolution. We linearly interpolated the data to 1 min resolution in order to obtain simultaneous field vectors at different spatial locations from the spacecraft. Magnetic field data from ACE were originally at 16 s resolution, Geotail and Wind data were at 3 s resolution, IMP 8 data were at 15 s resolution, and Interball data were at 6 s resolution. The selection of the solar wind intervals from these spacecraft could be automated because the intervals were long and plasma data were available from all spacecraft. The long life time of many of the spacecraft missions and their nearly constant immersion within the solar wind provided thousands of intervals for our study.

[22] One goal of this study is to show how the two-dimensional cross correlation function, $R(r_{\|}, r_{\perp})$, varies with the solar wind speed. For this purpose we binned the data into three different speed ranges: slow solar wind from about 250 to 450 km s^{-1}, fast solar wind for speeds greater than 600 km s^{-1}, and intermediate solar wind from 450 to 600 km s^{-1}. These speed ranges were selected to be similar to those specified in the study of *Dasso et al.* [2005] and to roughly equalize the number of intervals within each speed range. Approximately 2200 cross correlations values are available in the slow solar wind, 1200 values within the intermediate solar wind, and 1000 values within the fast solar wind.

3.1. Observations: Slow Solar Wind

[23] For each selected data interval, independent of the interval length, we calculate the time-averaged cross correlation of the magnetic field vector for each of the spacecraft pairs. This correlation value is assigned to a time-averaged separation distance for that interval in the directions parallel and perpendicular to the mean magnetic field. The mean was determined by averaging the magnetic field vector over the entirety of each interval (which ranged from one hour to 12 h duration, see previous section). Using the normalized cross correlation values from a large number of solar wind intervals, we obtain the two-dimensional, normalized correlation function as a function of spatial separation. The cross correlation values were normalized to the product of the root mean square values of the fluctuations of each component. With the correlation function we establish how the average

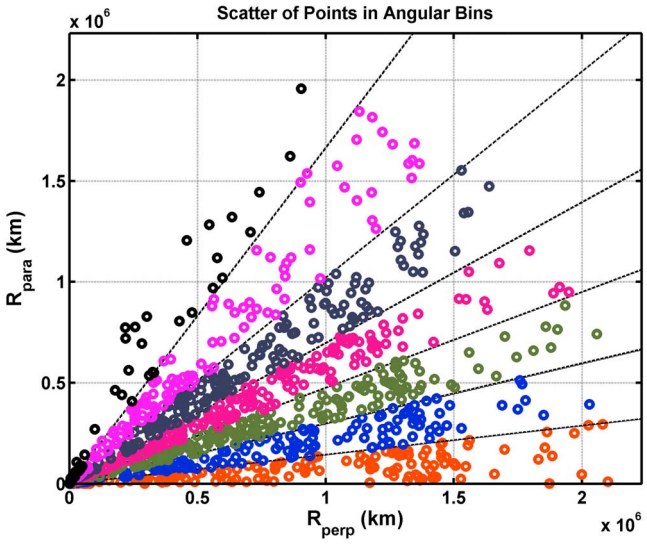

Figure 1. Scatterplot of absolute values of the spacecraft separations relative to the mean magnetic field direction. The dashed lines indicate the boundaries of seven angular bins subtending identical solid angle.

correlation scale and Taylor scale values depend on the solid angle relative to the background field. We assume that within each range of solar wind speeds the magnetic field turbulence in all angular bins has the same turbulence properties.

[24] Figure 1 displays the absolute value of the spacecraft separation in the parallel and perpendicular directions with respect to the mean magnetic field direction for intervals in the slow solar wind. In Figure 1, dashed lines show the boundaries of 7 different angular bins that are equally spaced solid angular bins of $\Delta\cos\theta = 0.143$. In the previous studies of *Weygand et al.* [2009, 2010] angular bins of 10° wide were used except for parallel spacecraft separation, which was 30° wide. Coincidently, the solid angle bins are nearly the same size as the angular bins and there is no difference between the results of this study and *Weygand et al.* [2009] within the uncertainty. Equal solid angle bins corresponding to equal surface areas were expected to provide roughly the same number of data intervals in each bin. However, in the parallel spacecraft separation bin in Figure 1 there are fewer data points than in the other bins.

[25] For each solid angular bin we used a least squares approach to fit the sum of two exponential functions to the data points to get the cross correlation (C) curve for that angular bin. The form used was

$$C = \beta \exp(-r/\lambda_{CS}) + (1-\beta)\exp(-r/\lambda_2) \qquad (2)$$

where β is a weighting term, r is the spacecraft separation, λ_{CS} and λ_2 are decay parameters. The uncertainties in these parameters were calculated from the residuals of the fit. We assume that the larger decay parameter is the turbulence correlation scale.

[26] Figure 2 displays the cross correlations from all angular bins versus spacecraft separation for slow solar wind speeds. All the slow solar wind cross correlation values were used in Figure 2 without separation into angular bins to demonstrate more clearly the need for two exponential functions in the fit. The light gray points show the cross correlations for each individual solar wind interval and the black diamonds are the means for spacecraft separation bins that range in size from hundreds of kilometers at small separations to millions of kilometers wide at larger separations. The vertical dashed lines mark the boundaries between the Cluster intervals, THEMIS intervals, and intervals established from other spacecraft pairs, respectively. The solid gray curve is a single exponential fit to the entire set of cross correlations versus spacecraft separation. The black dashed curve is the sum of two exponentials fit to the same data points. Figure 2 also shows that a single exponential function provided a good fit to the data available to *Matthaeus et al.* [2005], which included only very small and very large spatial separations. However, the new cross correlations, obtained from the larger Cluster spacecraft separations and the THEMIS pairs, show that a single exponential function is not a good fit to the cross correlation values.

[27] Figure 3 displays two-dimensional cross correlation functions determined using the sum of two exponentials and the single exponential fits to the separate angular bins. Figure 3 (top) shows the two-dimensional cross correlation function calculated from the sum of two exponential functions for each of the seven angular bins for the slow solar wind. The contours are obtained for only one quadrant of the plot and reflected to all other quadrants.

[28] Our results (Figure 3, top) do not resemble neither *Matthaeus et al.*'s [1990] Figure 3 nor *Dasso et al.*'s [2005] Figure 1a. However, those studies fitted single exponential functions to the correlation values. Another way in which to compare our results with the earlier work is to calculate a

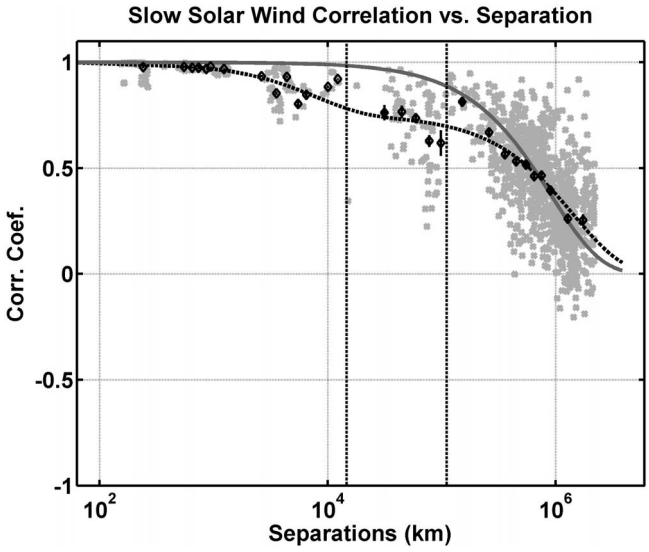

Figure 2. Cross correlations versus spacecraft separation for the slow solar wind. The gray points are the cross correlation points for the individual intervals. The black diamonds are means within spacecraft separation bins, and the error bars are the standard deviations. The vertical dashed lines separate the Cluster correlations from the THEMIS correlations and the THEMIS correlations from the remaining spacecraft correlations. The solid gray curve is a single exponential fit to the gray data points and the dashed black curve is a fit of the sum of two exponential functions.

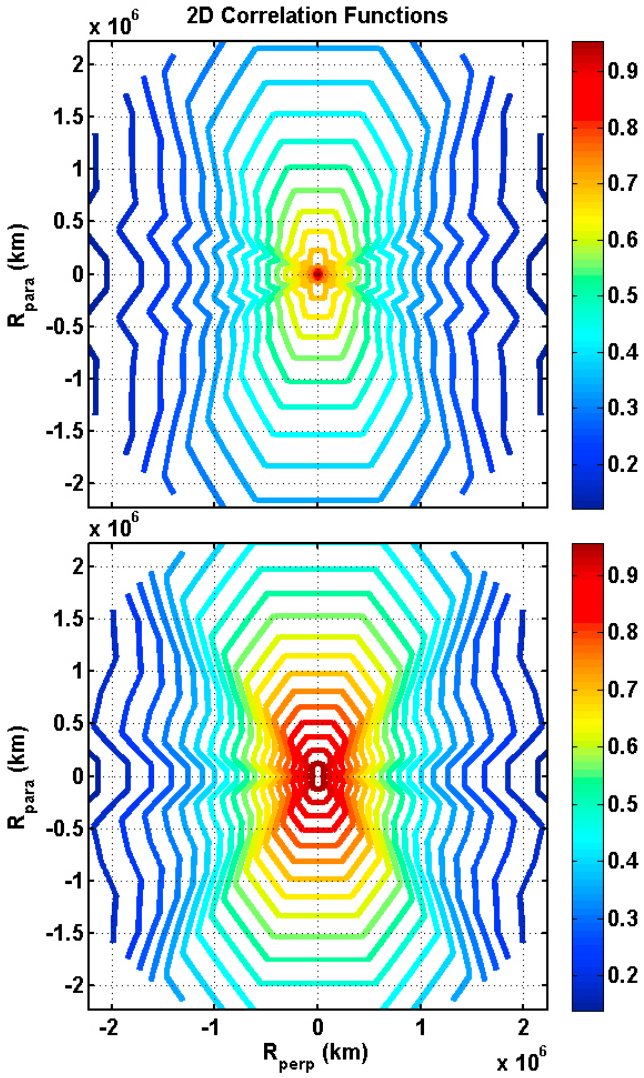

Figure 3. For the slow solar wind, (top) a two-dimensional correlation function versus distance along and across the average magnetic field direction from fits of data to the sum of two exponential functions. The color bar on the right-hand side of Figure 3 represents values of the cross correlation. (bottom) The two-dimensional correlation function obtained from excluding the second term in equation (2) for each angular bin and setting $\beta = 1$.

two dimensional contour plot using only a single exponential from our fit (the one with the longer decay length). For this purpose we exclude the second term in equation (2) for each angular bin, set β to 1, and use only the value obtained for λ_{CS}. Doing this we obtain the contours shown in Figure 3 (bottom), which is now similar to the plots of Matthaeus et al. and Dasso et al. We see in Figure 3 (bottom) as well as in Figure 1a of *Dasso et al.* [2005] and *Weygand et al.* [2009] that the correlation scale is longest along the mean magnetic field direction and shortest in the perpendicular direction. This procedure for producing the bottom images demonstrates that the Dasso et al. and *Weygand et al.* [2009] results are reproducible within this study, even though they are modified when data at intermediate separations are included. It is important to note that the equivalent distances covered in the Matthaeus et al. study are about twice as large as those in the lower illustration of their Figure 3 and that our Figure 3 covers distances approximately twice as large as those reported by *Dasso et al.*

[29] The parameters obtained by fitting equation (2) to the data in different angular bins are given in Tables 1, 2, and 3. The first two columns of these three tables give the angular range relative to the mean magnetic field direction and the solid angular range. The remaining three columns from left to right show the parameters obtained by fitting data for the slow, intermediate, and fast solar wind. The uncertainties given in the tables are the residuals of the least squares fit to the cross correlation data. Table 1 displays the correlation scale lengths λ_{CS} for each type of solar wind. Table 2 shows the second exponential decay length λ_2 and Table 3 tabulates the weighting parameter, β, (see equation (2)).

[30] The correlation scales for the slow solar wind shown in Table 1 show that the correlation scale is largest in the parallel direction and decreases relatively systematically with solid angle relative to the mean magnetic field as seen in Figure 3 (bottom). The slow solar wind magnetic field turbulence is anisotropic with a ratio of the correlation scale in the parallel direction to the perpendicular direction of 2.55 ± 0.76. However, Table 2 shows no clear systematic change of λ_2 with angle for the slow solar wind and only in the perpendicular bin does λ_2 differ significantly from values in the other angular bins. Table 3 shows that the value of β is 0.75 within twice the uncertainty for all but two of the solid angular bins for the slow solar wind.

[31] Table 4 has a similar format to Tables 1–3 and displays the Taylor scale values calculated for each angular bin in the three different solar wind speed ranges. The Taylor scale for each angular bin is found using a method based on the Richardson extrapolation technique [*Weygand et al.* 2007]. The technique estimates the radius of curvature of the cross correlation function at zero separation from a set of parabolic fits to the cross correlation values for small separations that are increased systematically until the radius of curvature (Taylor scale) becomes stable. The uncertain-

Table 1. Correlation Scale (λ_{CS}) for Each Solid Angular Bin for Each Range of Solar Wind Speed

Angle Relative to the Mean Magnetic Field	Solid Angle	Slow Solar Wind λ_{CS} (10^6) (km)	Intermediate Solar Wind λ_{CS} (10^6) (km)	Fast Solar Wind λ_{CS} (10^6) (km)
0.0°–31.0°	0.00–0.143	2.8 ± 0.8	2.8 ± 0.1	1.0 ± 0.2
31.0°–44.4°	0.143–0.286	2.3 ± 0.2	1.2 ± 0.1	1.1 ± 0.1
44.4°–55.1°	0.286–0.429	1.5 ± 0.1	1.2 ± 0.1	1.0 ± 0.1
55.1°–64.6°	0.429–0.571	1.3 ± 0.1	1.2 ± 0.1	1.1 ± 0.1
64.6°–73.4°	0.571–0.714	1.3 ± 0.1	1.0 ± 0.1	1.9 ± 0.8
73.4°–81.8°	0.714–0.857	1.3 ± 0.1	1.2 ± 0.1	1.8 ± 0.6
81.8°–90.0°	0.857–1.00	1.1 ± 0.1	1.3 ± 0.1	1.4 ± 0.5

Table 2. Small Decay Length (λ_2) for Each Solid Angular Bin for Each Range of Solar Wind Speed

Angle Relative to the Mean Magnetic Field	Solid Angle	Slow Solar Wind λ_2 (10^3) (km)	Intermediate Solar Wind λ_2 (10^3) (km)	Fast Solar Wind λ_2 (10^3) (km)
0.0°–31.0°	0.00–0.143	20.2 ± 8.7	10.7 ± 6.1	0.7 ± 13.1
31.0°–44.4°	0.143–0.286	26.9 ± 5.7	1.1 ± 1.3	1.3 ± 1.3
44.4°–55.1°	0.286–0.429	14.0 ± 3.6	9.4 ± 4.0	25.0 ± 22.2
55.1°–64.6°	0.429–0.571	8.8 ± 2.4	12.9 ± 3.7	19.5 ± 12.0
64.6°–73.4°	0.571–0.714	30.4 ± 6.9	6.3 ± 2.6	150.3 ± 54.9
73.4°–81.8°	0.714–0.857	11.7 ± 3.1	13.1 ± 4.4	94.1 ± 41.1
81.8°–90.0°	0.857–1.00	8.3 ± 2.5	16.2 ± 4.7	106.9 ± 61.4

ties given are the standard deviations obtained from the Richardson extrapolation technique [*Weygand et al.* 2007]. Note that the Taylor scale estimates are determined here from the trace of the two-point magnetic autocorrelation near the origin and therefore are not sensitive to the random (and intermittent) fluctuations of the anisotropy of vector component variances that are measured at these small scales [see, e.g., *Perri et al.*, 2009].

[32] The Taylor scales in the slow solar wind do not vary systematically with angle; all values lie within two standard deviations of each other.

[33] In summary for the slow solar wind only the correlation scales show a clear systematic variation with the mean magnetic field direction while the second exponential decay length, weight term, and Taylor scale show no clear variation with solid angle.

3.2. Observations: Fast Solar Wind and Intermediate Solar Wind

[34] For the intermediate and fast solar wind we repeat the procedures applied to the slow solar wind in section 3.1, which was to first fit the angular bins with the sum of two exponential functions and then use the results for the correlation scales to calculate the two-dimensional correlation function from single exponential functions. Figures 4 and 5 show the two-dimensional correlation functions obtained from fitting the sum of two exponential functions to the solid angular bins (top) and the two-dimensional correlation functions obtained from the single exponential fits using the correlation scales from the fits (bottom). The contours for the intermediate solar wind in Figure 4 show that the correlation scale is longer in the parallel direction than in the perpendicular direction. In Figure 5 (top) the contours for the fast solar wind are longest in the parallel direction, but when we consider only the correlation scales in Figure 5 (bottom) for the fast solar wind, the correlation scale is longest in the direction perpendicular to the mean magnetic field direction and shorter in the parallel direction, although the uncertainties on these length scales are large.

[35] The correlation scales for the intermediate and fast solar wind listed in Table 1 show that the parallel correlation scale decreases as the solar wind speed increases. An increase with solar wind speed of the mean correlation scale in the perpendicular direction is suggested, but the perpendicular correlation scales do not differ within the uncertainties given in Table 1. Table 1 also shows the correlation scale in the intermediate solar wind (fourth column) is longer in the parallel angular bin than perpendicular angular bins. The ratio of the parallel correlation scale to the perpendicular correlation scale is 2.15 ± 0.18, which is similar to the slow solar wind anisotropy. The change of the correlation scale with angle in the fast solar wind (fifth column) is not clear because the uncertainties are large. The ratio to the parallel to perpendicular correlation scales for the fast solar wind is 0.71 ± 0.29, which is smaller than the ratio for the slow and intermediate solar wind.

[36] In Table 2, uncertainties again mask any clear change in the second decay length (λ_2) for the intermediate solar wind. However, the second decay length increases from the parallel bin to the perpendicular bin for the fast solar wind.

[37] The weighting factor (β) for the intermediate and fast solar wind in Table 3 are for the most part close to the values in the slow solar wind. In the intermediate solar wind β is approximately 0.75 within twice the uncertainty for all but two of the solid angular bins. However, in the fast solar wind the average β is 0.64 and its value varies between 0.42 and 0.97. The large range of values for β in the fast solar wind fits is most likely related to the limited number of cross correlation values in each solid angular bin.

[38] The Taylor scales, like the correlation scales shown in Table 4, are larger in the parallel direction than in the perpendicular direction in the intermediate solar wind. However, no systematic variation is observed in the Taylor scales for the fast solar wind, possibly because of the absence of data at small scale separations indicated by the

Table 3. Weight Parameter (β) for Each Solid Angular Bin for Each Range of Solar Wind Speed

Angle Relative to the Mean Magnetic Field	Solid Angle	Slow Solar Wind (β)	Intermediate Solar Wind (β)	Fast Solar Wind (β)
0.0°–31.0°	0.00–0.143	0.81 ± 0.03	0.76 ± 0.05	0.97 ± 0.11
31.0°–44.4°	0.143–0.286	0.75 ± 0.04	0.87 ± 0.02	0.78 ± 0.04
44.4°–55.1°	0.286–0.429	0.69 ± 0.3	0.75 ± 0.04	0.68 ± 0.05
55.1°–64.6°	0.429–0.571	0.79 ± 0.02	0.71 ± 0.03	0.60 ± 0.04
64.6°–73.4°	0.571–0.714	0.77 ± 0.03	0.77 ± 0.04	0.42 ± 0.09
73.4°–81.8°	0.714–0.857	0.72 ± 0.02	0.70 ± 0.04	0.46 ± 0.06
81.8°–90.0°	0.857–1.00	0.75 ± 0.07	0.65 ± 0.04	0.52 ± 0.09

Table 4. Taylor Scale (λ_{TS}) for Each Solid Angular Bin for Each Range of Solar Wind Speed[a]

Angle Relative to the Mean Magnetic Field	Solid Angle	Slow Solar Wind λ_{TS} (10^3) (km)	Intermediate Solar Wind λ_{TS} (10^3) (km)	Fast Solar Wind λ_{TS} (10^3) (km)
0.0°–31.0°	0.00–0.143	1.4 ± 0.2	3.5 ± 0.5	NA (0)
31.0°–44.4°	0.143–0.286	0.4 ± 0.4	0.9 ± 0.5	0.7 ± 0.4 (7)
44.4°–55.1°	0.286–0.429	1.5 ± 0.2	1.3 ± 0.2	0.6 ± 1.4 (2)
55.1°–64.6°	0.429–0.571	1.5 ± 0.7	1.4 ± 0.3	1.3 ± 0.04 (9)
64.6°–73.4°	0.571–0.714	0.9 ± 0.2	0.8 ± 0.4	1.3 ± 0.04 (8)
73.4°–81.8°	0.714–0.857	1.4 ± 0.2	2.5 ± 0.2	0.4 ± 1.0 (6)
81.8°–90.0°	0.857–1.00	1.4 ± 0.1	1.2 ± 0.5	1.1 ± 0.1 (6)

[a]The numbers in parentheses in the last column are the number of data points used in determination of the fast solar wind Taylor scale.

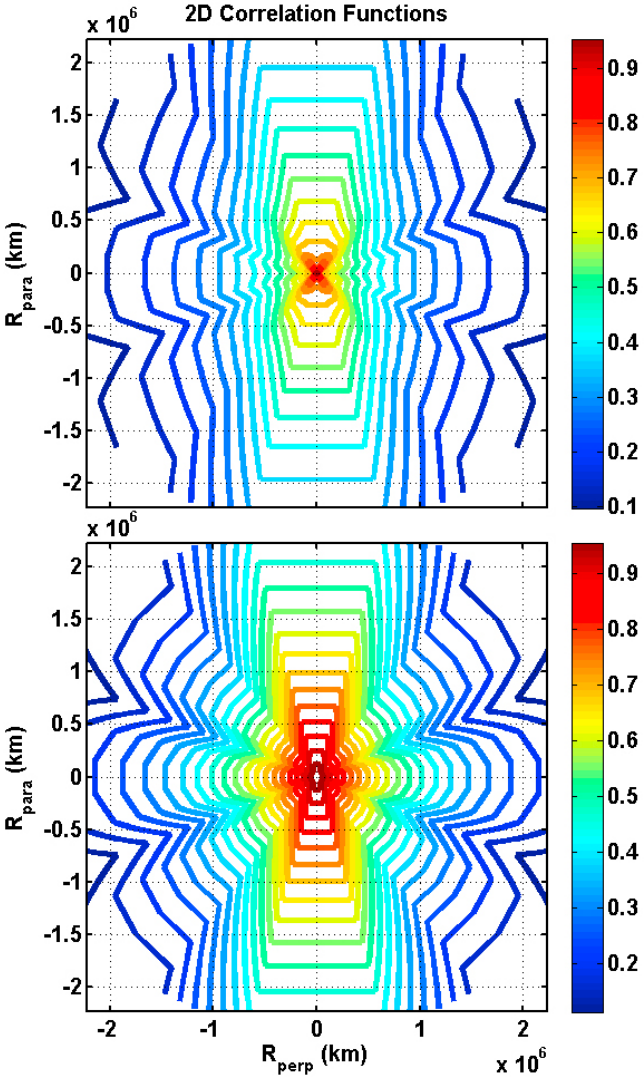

Figure 4. Two-dimensional correlation functions for the intermediate solar wind. Figure 4 has the same format as Figure 3. (top) The contours obtained from the sum of to exponentials function fits and (bottom) the contours obtained from the single exponential functions.

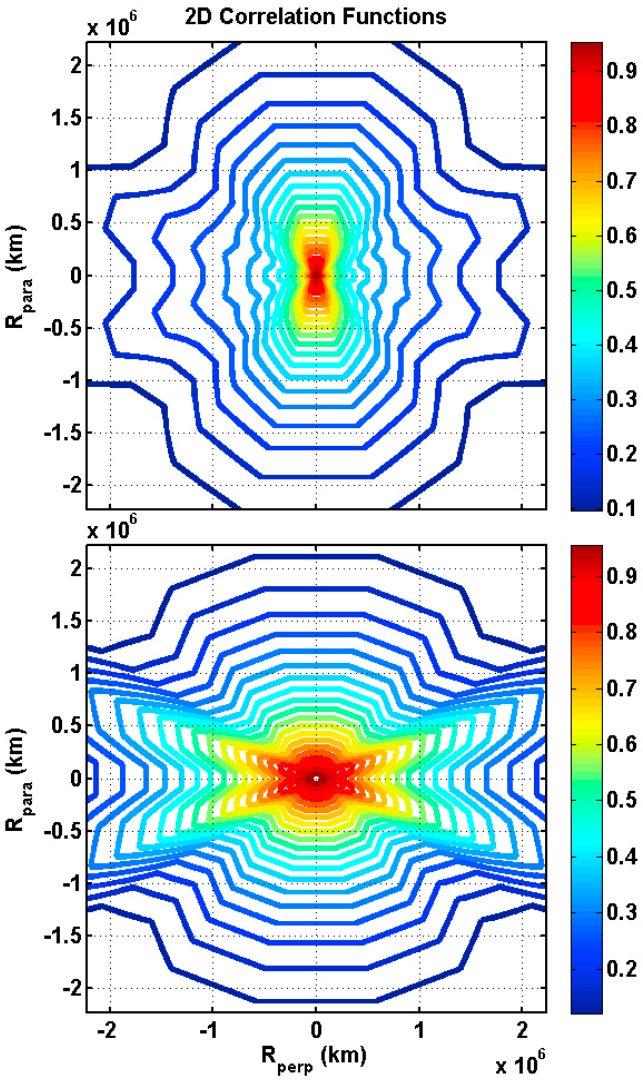

Figure 5. Two-dimensional correlation functions for the fast solar wind. Figure 5 has the same format as Figure 3. (top) The contours obtained from the sum of two exponentials function fits and (bottom) the contours obtained from the single exponential functions.

number within the parentheses shown in the last column of Table 4.

4. Discussion

[39] Tables 1 and 4 and Figures 3, 4, and 5 showed of the dependence of the correlation and the Taylor scales with angle relative to the average magnetic field in different ranges of solar wind speed (slow, intermediate, and fast). We caution the reader, when considering the discussion of the results, to be cognizant of the substantial fractional errors associated with some of the tabulated results, especially the estimated Taylor scales and effective Reynolds numbers.

[40] Some of the reported angular and speed variations have been reported in previous studies such as *Matthaeus et al.* [1990], *Dasso et al.* [2005], *Osman and Horbury* [2007], and *Weygand et al.* [2009]. Matthaeus et al. displayed two-dimensional correlation contours with a Maltese cross shape with the longest correlation length perpendicular to the mean magnetic field and attributed that pattern to a superposition of quasi two-dimensional and slab-like solar wind turbulence. Their correlation contours did not differentiate ranges of solar wind speed. Dasso et al. reported autocorrelation values for two different solar wind speed ranges: slow solar wind (<400 km s^{-1}) and fast solar wind (>500 km s^{-1}). They found the correlation scale longest along the mean magnetic field and shortest perpendicular to it in the slow solar wind and the reverse in the fast solar wind. In this study we also obtain results characteristic of the two different types of solar wind turbulence, but, by also examining solar wind of intermediate speeds, we are also able to identify a transition from the dominance of quasi two-dimensional turbulence in the slow solar wind, where the correlation scale is longest along the mean magnetic field, to the dominance of mainly slab like turbulence in the fast solar wind, where the correlation scale is longest in the perpendicular direction. Furthermore, we have enough cross correlations over a wide range of separations, including separations smaller than the Taylor scale, to be able to calculate the Taylor scale for each solar wind speed range and solid angular bin except in the 0 to 0.143 solid angular bin in the fast solar wind.

[41] In this study we have used the same method as *Osman and Horbury* [2007], and *Weygand et al.* [2009] to quantify the anisotropy observed in the solar wind magnetic field turbulence. That method consists of determining the ratio of the correlation scale in the direction parallel to the mean magnetic field to the perpendicular direction. *Osman and Horbury* [2007], using time-lagged two-point correlations obtained from the x and z components of the Cluster magnetic field data from a single slow solar wind interval, found an anisotropy ratio of 1.79 ± 0.36 using a spatial autocorrelation function. The fact that the correlations are longest along the magnetic field suggests that the solar wind includes a substantial contribution from quasi two-dimensional fluctuations, for which a leading order description is the two-dimensional model. That is to say, the bulk of the fluctuations appear to be from quasi two-dimensional turbulent fluctuations in the slow solar wind. *Weygand et al.* [2009], which like this study, used spacecraft pairs to examine the anisotropy of the turbulence correlation scale within the slow solar wind, found that the ratio of the parallel correlation scale to the perpendicular correlation scale was 2.62 ± 0.79. The ratio found here for the slow solar wind is 2.55 ± 0.76, which is consistent with *Osman and Horbury* within the uncertainty, but closer in magnitude to the value reported by of *Weygand et al.* [2009]. The similarity to *Weygand et al.* [2009] is not surprising because there is considerable overlap of the data sets used. We interpret the relatively large value of the anisotropy to mean that the slow solar wind consists mainly of quasi two-dimensional fluctuations.

[42] *Weygand et al.* [2009] also extracted the anisotropy ratio from the two-dimensional correlation contours given in the work by *Matthaeus et al.* [1990] and *Dasso et al.* [2005] for the slow solar wind and found much smaller values of 0.9 and 1.2, respectively, The anisotropy ratio identified from Matthaeus et al. is smaller than other reported values, probably because it includes data from a wide range of solar wind speeds. *Weygand et al.* [2009] suggested that the anisotropy ratio in the slow solar wind reported by Dasso et al. was smaller than that found by *Weygand et al.* [2009] because the two studies used different angular bin sizes which was 22.5° in all directions for Dasso et al. compared to 30° in the direction parallel to the mean magnetic field and 10° in the perpendicular direction for Weygand et al. Differing bin sizes were used by *Weygand et al.* [2009] because of the limited number of data points in the parallel bin. However, the *Weygand et al.* [2009] study showed that the anisotropy ratio for slow solar wind did not vary when the range of slow solar wind speeds considered was changed slightly. In any case, the ratios found in both the Matthaeus et al. and Dasso et al. papers are much smaller than the ratio determined by *Weygand et al.* [2009].

[43] In addition to the anisotropy ratio for the slow solar wind, *Dasso et al.* [2005] calculated the anisotropy ratio for the fast solar wind, finding it to be 0.71. In the present work, we find that the anisotropy of the fast solar wind is 0.71 ± 0.29. This result agrees with the results of Dasso et al. despite the differences the angular bin size and in the solar wind speed range considered, which was >500 km s^{-1} in the work given by Dasso et al. and >600 km s^{-1} in this study. As contrasted with earlier work, in this study we have characterized not only slow solar wind and fast solar wind but also the intermediate solar wind for which we find an anisotropy of 2.15 ± 0.18. This value is interesting because it lies between values found for the slow solar wind and fast solar wind and suggests a monotonic transition from one type of solar wind turbulence to another.

[44] In Table 4 we give the Taylor scale calculated in each solar wind speed range and angular bin. In the slow solar wind, there is no significant variation of the Taylor scale with solid angle relative to the mean magnetic field direction. Within the fast solar wind, we cannot establish anisotropy in the Taylor scales, because we lack data in the parallel angular bin. However, in the intermediate solar wind we do observe some anisotropy. The ratio of the parallel to perpendicular Taylor scales is 2.91 ± 1.28. This ratio is the same within uncertainty to the anisotropy ratio in the correlation scales for the intermediate solar wind, but the uncertainty for the Taylor scale anisotropy ratio is rather large. One might be tempted to believe that the anisotropy for these two turbulence scale lengths suggests that the

Table 5. Effective Magnetic Reynolds Numbers for Each Solid Angular Bin for Each Range of Solar Wind Speed

Angle Relative to the Mean Magnetic Field	Solid Angle	Slow Solar Wind (10^6)	Intermediate Solar Wind (10^6)	Fast Solar Wind (10^6)
0.0°–31.0°	0.00–0.143	4.0 ± 3.7	0.6 ± 0.5	NA
31.0°–44.4°	0.143–0.286	31.7 ± 44.4	1.9 ± 1.5	2.7 ± 3.2
44.4°–55.1°	0.286–0.429	1.1 ± 0.7	0.9 ± 0.8	2.9 ± 6.3
55.1°–64.6°	0.429–0.571	0.8 ± 0.4	0.8 ± 0.6	0.7 ± 0.3
64.6°–73.4°	0.571–0.714	2.2 ± 1.6	1.5 ± 1.7	2.0 ± 2.0
73.4°–81.8°	0.714–0.857	0.9 ± 0.6	0.2 ± 0.2	22.6 ± 57.5
81.8°–90.0°	0.857–1.00	0.6 ± 0.3	1.3 ± 1.5	1.5 ± 1.4

correlation scale anisotropy is imposed upon the Taylor scales. However, since the anisotropy ratio for the Taylor scale in the slow solar wind (1.0 ± 0.16) is significantly different from the anisotropy ratio of the slow solar wind correlation scales this proposal must be rejected. The reason anisotropy is observed in the Taylor scales for intermediate solar wind, but not in the slow solar wind, is not clear at this time.

[45] Equation (1) enables us to calculate the effective magnetic Reynolds number for each angular bin (Table 5) for each solar wind speed range. Because of the large uncertainties in derived quantities, the tabulated data do not clearly show that the effective magnetic Reynolds number varies with solid angle for the slow and intermediate solar wind. The effective magnetic Reynolds number may vary with solid angle in the fast solar wind, but the evidence rests on a single, uncertain data point determined from a small number of Taylor scale observations (see the value in the parenthesis in the fifth column of Table 4). We find an effective magnetic Reynolds number of a few million represents the bulk of the tabulated values within twice the uncertainty for all solar wind speed ranges combined. The mean effective magnetic Reynolds number from Table 5 is about 4.0×10^6 with a range from 0.2 to 31×10^6. Thus all of the present estimates are considerably larger than the values given by *Matthaeus et al.* [2005] ($\sim 2.3 \cdot 10^5$) and *Weygand et al.* [2007] ($\sim 2.6 \pm 0.2 \times 10^5$). However, these values are consistent with those found by *Weygand et al.* [2009]. The differences can be attributed principally to the different values obtained for the Taylor scale in the present study.

[46] *Matthaeus et al.* [2005] fit the correlation versus separation data with a single exponential. Cluster and THEMIS measurements not available to *Matthaeus et al.* [2005] demonstrate that the data cannot be well fit by a single exponential and a more complicated function is required (see Figure 2). For this study we have used the sum of two exponentials as a more appropriate function. From the double exponential fit we obtain three values: a first decay value (Table 1), a second decay value (Table 2), and a weighting factor (Table 3). We have assumed that the largest decay value is the correlation scale associated with the largest turbulent eddy scale sizes. However, the physical meaning of the second decay parameter is unclear. *Weygand et al.* [2009] found that the fits to the data indicate that the largest decay length is determined with the largest spacecraft separations (i.e., those among ACE, Geotail IMP 8, Interball, and Wind) while the smaller decay length is established with smaller spacecraft separations among just the Cluster spacecraft pairs. In this study we use not only Cluster but also a number of intervals provided by THEMIS data and these data show that the additional exponential term with a second shorter decay length (λ_2) is required to fit a portion of the THEMIS data. With the new THEMIS data we are able to establish that the second decay length does not result from instrumental bias associated with the Cluster data. However, in addition to their separations, the most significant difference between the ACE, Geotail IMP 8, Interball, and Wind spacecraft and the Cluster and THEMIS spacecraft is that when Cluster and THEMIS are in the solar wind, they are sometimes in the foreshock region.

[47] An alternative explanation for the second (smaller) decay length was suggested by *Borovsky* [2008], who proposed that the solar wind is composed of distinguishable flux tubes and that the turbulent magnetic fluctuations are localized within those flux tubes. They showed that within the solar wind there are two populations of magnetic field rotations, one population for small rotations at small spatial separations and one population for large rotations at larger spatial separation. Based on this idea, the large scale length could be associated with the mean flux tube diameter of 1.4×10^6 km, which is very similar to our mean correlation scale of 1.5×10^6 km calculated from all the correlation scales in Table 1. The smaller decay length then would be the large eddy scale size (about the correlation scale size) of turbulent fluctuations within the flux tube, which is about 1.4×10^5 km. The mean small decay length in our study is about 30,000 km, which is about a factor of 5 smaller than the eddy scale size reported by *Borovsky* [2008]. This difference is relatively large, but the large eddy scale size determined by *Borovsky* [2008] appears to be arbitrary. Furthermore, it is unclear how we could test the *Borovsky* [2008] hypothesis.

[48] Similar to the Borovsky et al. study, *Greco et al.* [2009] examined the distribution of waiting times between magnetic discontinuities in the ACE magnetic field data. They found that this distribution was best fit with a power law at scales smaller than the correlation scale, which they assume was 1.2×10^6 km [*Greco et al.*, 2008], and at larger scales the distribution was best fit with an exponential. According to *Greco et al.* [2009], the discontinuities may represent the current sheets that form between magnetic flux tubes that have correlation scale as the typical dimension. These current structures form a hierarchy that extends through the upper part of inertial range to its termination near the dissipation scale. The latter is often taken to be near the ion inertial scale, which is also a characteristic scale of thinned current sheets in collisionless reconnection [*Leamon et al.*, 2000]. The relationship between dissipation scale and Taylor scale in the solar wind is more complex than it is in

hydrodynamics, and in some fraction of cases the Taylor scale is found to be smaller than the dissipation scale [*Matthaeus et al.*, 2008] in contrast to hydrodynamic turbulence at high Reynolds number. Consequently while it is clear that dynamical relationships exist among the Taylor, dissipation and current sheet thickness scales, it is also clear that these relationships are not well understood and remain topics of current and ongoing research. The same comments apply to the possible relationship between the second exponential decay length we introduced on empirical grounds, and the properties of the cascade and current sheets discussed by Greco et al. Further investigation is required to clarify these relationships.

5. Summary and Conclusions

[49] In this study we examined the correlation and Taylor scales as functions of the solid angle relative to the mean magnetic field direction in slow, intermediate, and fast solar wind speed ranges. As far as we are aware this is the first study to use only simultaneous two point correlation measurements to determine the variation of these scales of turbulent fluctuations with respect to the mean magnetic field for solar wind of different speeds. We find that within the intermediate solar wind, the Taylor scale is longest along the magnetic field (~3500 ± 500 km) and shorter perpendicular to the magnetic field (~1200 ± 500 km). Finding that the Taylor scale depends on direction in the intermediate solar wind is puzzling in view of the fact that, to within uncertainty, we found no directional dependence in the slow or fast solar wind. The differences may involve some elements of anisotropy related to dispersive and dissipative effects at small scale lengths or may be related to anisotropy at the inertial range scales imposed upon the Taylor scales.

[50] Using the Taylor scale and the correlation scale, we derived the effective magnetic Reynolds number for each angular bin. In all three solar wind speed ranges, the effective magnetic Reynolds number shows some variability with solid angle relative to the magnetic field, but remains within 2 standard deviations of a typical value of a few million. A study using a larger data set will be needed to establish whether there is an angular variation of the effective magnetic Reynolds number.

[51] Our results show that the correlation scale is longest along the magnetic field and shorter perpendicular to the magnetic field in both the slow solar wind and the intermediate solar wind with the difference larger in the slow solar wind. The ratios of the parallel to the perpendicular correlation scales were found to be 2.55 ± 0.76 and 2.15 ± 0.18 for the slow solar wind and the intermediate solar wind, respectively. These values agree (within the uncertainty) with the single value reported by *Osman and Horbury* [2007] for a slow solar wind interval. In the fast solar wind, the ratio is 0.71 ± 0.29, the same as the ratio reported by *Dasso et al.* [2005]. This monotonic transition from a large anisotropy in the slow solar wind to a value a little less than 1 in the fast solar wind suggests that quasi two-dimensional turbulence dominates within the slow solar wind, but that the dominance gradually decreases until Alfvénic turbulence dominates within the fast solar wind. The fact that the correlation scale varies with respect to the mean magnetic field direction is important to studies of solar and galactic cosmic ray scattering that depend on accurate determination of the perpendicular diffusion coefficient, which is directly proportional to the correlation scale [*Ruffolo et al.*, 2004].

[52] **Acknowledgments.** This work was supported by NASA grant NAG5–12131 and NSF grant ATM-0702916 at UCLA. W.H. Matthaeus is partially supported by NSF grants ATM-0539995 and ATM-0752135 (SHINE), and by NASA NNX08AI47G and NNG05GG83G at the University of Delaware. S. Dasso thanks the Argentinean grants: UBACyT X425 (UBA) and 03–33370 (ANPCyT). S. Dasso is a member of the Carrera del Investigador Científico (CONICET). We would like to thank M.L. Goldstein, J.E. Borovsky, and Z. Vörös for their helpful discussions. We would also like to thank H. Schwarzl and K.K. Khurana for calibrating the Cluster magnetometer data and their advice on the calibration process. We would also like to thank U. Auster for calibrating the THEMIS magnetometer data and his advice on the calibration process. Finally, we thank E. Lucek for providing UCLA with the Cluster magnetometer data.

[53] Philippa Browning thanks the reviewers for their assistance in evaluating this paper.

References

Auster, H. U., et al. (2008), The THEMIS fluxgate magnetometer, *Space Sci. Rev.*, *141*, 235–264, doi:10.1007/s11214-008-9365-9.

Balogh, A., et al. (1997), The Cluster magnetic field investigation, *Space Sci. Rev.*, *79*, 65–91, doi:10.1023/A:1004970907748.

Batchelor, G. K. (1970), *Theory of Homogeneous Turbulence*, Cambridge Univ. Press, Cambridge, U. K.

Bieber, J. W., W. H. Matthaeus, C. W. Smith, W. Wanner, M.-B. Kallenrode, and G. Wibberenz (1994), Proton and electron mean free paths: The Palmer consensus revisited, *Astrophys. J.*, *420*, 294–306, doi:10.1086/173559.

Bieber, J. W., W. Wanner, and W. H. Matthaeus (1996), Dominant two-dimensional solar wind turbulence with implications for cosmic ray transport, *J. Geophys. Res.*, *101*, 2511–2522, doi:10.1029/95JA02588.

Borovsky, J. E. (2008), Flux tube texture of the solar wind: strands of the magnetic carpet at 1 AU?, *J. Geophys. Res.*, *113*, A08110, doi:10.1029/2007JA012684.

Borovsky, J. E., R. C. Elphic, H. O. Funsten, and M. F. Thomsen (1997), The Earth's plasma sheet as a laboratory for turbulence in high-beta MHD, *J. Plasma Phys.*, *57*, 1–34, doi:10.1017/S0022377896005259.

Burlaga, L. F. (1991a), Multifractal structure of the interplanetary magnetic field: Voyager 2 observations near 25 AU, 1987-1988, *Geophys. Res. Lett.*, *18*, 69–72, doi:10.1029/90GL02596.

Burlaga, L. F. (1991b), Multifractal structure of speed fluctuations in recurrent streams at 1 AU and near 6 AU, *Geophys. Res. Lett.*, *18*, 1651–1654, doi:10.1029/91GL01221.

Burlaga, L. F. (1991c), Intermittent turbulence in the solar wind, *J. Geophys. Res.*, *96*, 5847–5851, doi:10.1029/91JA00087.

Burlaga, L. F., and L. W. Klein (1986), Fractal structure of the interplanetary magnetic field, *J. Geophys. Res.*, *91*, 347–350, doi:10.1029/JA091iA01p00347.

Dasso, S., L. J. Milano, W. H. Matthaeus, and C. W. Smith (2005), Anisotropy in fast and slow solar wind fluctuations, *Astrophys. J.*, *635*, L181–L184, doi:10.1086/499559.

Duffy, P., and K. M. Blundell (2005), Cosmic ray transport and acceleration, *Plasma Phys. Controlled Fusion*, *47*, B667, doi:10.1088/0741-3335/47/12B/S49.

Escoubet, C. P., R. Schmidt, and M. L. Goldstein (1997), Cluster-science and mission overview, *Space Sci. Rev.*, *79*, 11–32, doi:10.1023/A:1004923124586.

Frank, L. A., K. L. Ackerson, W. R. Paterson, J. A. Lee, M. R. English, and G. L. Pickett (1994), The Comprehensive Plasma Instrumentation (CPI) for the Geotail spacecraft, *J. Geomag. Geoelectr.*, *46*, 23–37, doi:10.5636/jgg.46.23.

Gazis, P. R., A. Barnes, J. D. Mihalov, and A. J. Lazarus (1994), Solar wind velocity and temperature in the outer heliosphere, *J. Geophys. Res.*, *99*, 6561–6573, doi:10.1029/93JA03144.

Goldstein, M. L., D. A. Roberts, and C. A. Fitch (1994), Properties of the fluctuating magnetic helicity in the inertial and dissipation ranges of solar wind turbulence, *J. Geophys. Res.*, *99*, 11,519–11,538, doi:10.1029/94JA00789.

Goldstein, M. L., D. A. Roberts, and W. H. Matthaeus (1995), Magnetohydrodynamic turbulence in the solar wind, *Annu. Rev. Astron. Astrophys.*, *33*, 283–325, doi:10.1146/annurev.aa.33.090195.001435.

Greco, A., P. Chuychai, W. H. Matthaeus, S. Servidio, and P. Dmitruk (2008), Intermittent MHD structures and classical discontinuities, *Geophys. Res. Lett.*, *35*, L19111, doi:10.1029/2008GL035454.

Greco, A., W. H. Matthaeus, S. Servidio, and P. Dmitruk (2009), Waiting-time distributions of magnetic discontinuities: Clustering or Poisson process?, *Phys. Rev. E*, *80*, 046401, doi:10.1103/PhysRevE.80.046401.

Kokubun, S., T. Yamamoto, M. H. Acuna, K. Hayashi, K. Shiokawa, and H. Kawano (1994), The Geotail magnetic field experiment, *J. Geomag. Geoelectr.*, *46*, 7–21, doi:10.5636/jgg.46.7.

Kolmogorov, A. N. (1941), The local structure of turbulence in incompressible viscous fluid for very large Reynolds' numbers, *Dokl. Akad. Nauk SSSR*, *30*, 301–305.

Kraichnan, R. H. (1965), Inertial-range spectrum of hydromagnetic turbulence, *Phys. Fluids*, *8*, 1385, doi:10.1063/1.1761412.

Lazarus, A. J., and K. I. Paularena (1998), A comparison of solar wind parameters from experiments on the IMP 8 and Wind spacecraft, in *Measurement Techniques in Space Plasmas*, *Geophys. Monogr. Ser.*, vol. 102, edited by J. E. Borovsky, R. F. Pfaff, and D. T. Young, pp. 85–90, AGU, Washington, D. C.

Leamon, R. J., W. H. Matthaeus, C. W. Smith, G. P. Zank, and D. J. Mullan (2000), MHD driven kinetic dissipation in the solar wind and corona, *Astrophys. J.*, *537*, 1054, doi:10.1086/309059.

Lepping, R. P., et al. (1995), The WIND magnetic field investigation, *Space Sci. Rev.*, *71*, 207–229, doi:10.1007/BF00751330.

Lin, R. P., et al. (1995), A three-dimensional plasma and energetic particle investigation for the Wind spacecraft, *Space Sci. Rev.*, *71*, 125–153, doi:10.1007/BF00751328.

Matthaeus, W. H., M. L. Goldstein, and D. A. Roberts (1990), Evidence for the presence of quasi-two-dimensional nearly incompressible fluctuations in the solar wind, *J. Geophys. Res.*, *95*, 20,673–20,683, doi:10.1029/JA095iA12p20673.

Matthaeus, W. H., S. Dasso, J. M. Weygand, L. J. Milano, C. W. Smith, and M. G. Kivelson (2005), Spatial correlation of the solar wind turbulence from two point measurements, *Phys. Rev. Lett.*, *95*, 231101, doi:10.1103/PhysRevLett.95.231101.

Matthaeus, W. H., J. M. Weygand, P. Chuychai, S. Dasso, C. W. Smith, and M. G. Kivelson (2008), Interplanetary magnetic Taylor scale and implications for plasma dissipation, *Astrophys. J.*, *678*, L141, doi:10.1086/588525.

McComas, D. J., S. J. Bame, P. Barker, W. C. Feldman, J. L. Phillips, P. Riley, and J. W. Griffee (1998), Solar Wind Electron Proton Alpha Monitor (SWEPAM) for the Advanced Composition Explorer, *Space Sci. Rev.*, *86*, 563–612, doi:10.1023/A:1005040232597.

McFadden, J. P., C. W. Carlson, D. Larson, M. Ludham, R. Abiad, B. Elliott, P. Turin, M. Marckwordt, and V. Angelopoulos (2008), The THEMIS, ESA plasma instrument and in-flight calibration, *Space Sci. Rev.*, *141*, 277–302, doi:10.1007/s11214-008-9440-2.

Milano, L. J., W. H. Matthaeus, P. Dmitruk, and D. C. Montgomery (2001), Local anisotropy in incompressible magnetohydrodynamic turbulence, *Phys. Plasmas*, *8*, 2673, doi:10.1063/1.1369658.

Mukai, T., S. Machida, Y. Saito, M. Hirahara, T. Terasawa, N. Kaya, T. Obara, M. Ejiri, and A. Nishida (1994), The low energy particle (LEP) experiment onboard the Geotail satellite, *J. Geomag. Geoelectr.*, *46*, 669–692, doi:10.5636/jgg.46.669.

Nozdrachev, M. N., V. A. Styazhkin, A. A. Zarutsky, S. I. Klimov, S. P. Savin, A. A. Skalsky, A. A. Petrukovich, Y. V. Lissakov, I. S. Arshinkov, N. Abadgiev, and A. Bochev (1995), Magnetic field measurements onboard the Interball tail spacecraft: The FM-3I instrument, in *Interball Mission and Payload*, pp. 228–229, CNES, Toulouse, France.

Osman, K. R., and T. S. Horbury (2007), Multispacecraft measurement of anisotropic correlation functions in the solar wind turbulence, *Astrophys. J.*, *654*, L103–L106, doi:10.1086/510906.

Oughton, S., and W. H. Matthaeus (2005), Parallel and perpendicular cascades in solar wind turbulence, *Nonlinear Process. Geophys.*, *12*, 299–310, doi:10.5194/npg-12-299-2005.

Perri, S., E. Yordanova, V. Carbone, P. Veltri, L. Sorriso-Valvo, R. Bruno, and M. André (2009), Magnetic turbulence in space plasmas: Scale-dependent effects of anisotropy, *J. Geophys. Res.*, *114*, A02102, doi:10.1029/2008JA013491.

Rème, H., et al. (1997), The Cluster ion spectrometry (CIS) experiment, *Space Sci. Rev.*, *79*, 303–350, doi:10.1023/A:1004929816409.

Richardson, J. D., and C. W. Smith (2003), The radial temperature profile of the solar wind, *Geophys. Res. Lett.*, *30*(5), 1206, doi:10.1029/2002GL016551.

Richardson, J. D., K. L. Paularena, A. J. Lazarus, and J. W. Belcher (1995), Radial evolution of the solar wind from IMP 8 to Voyager 2, *Geophys. Res. Lett.*, *22*, 325, doi:10.1029/94GL03273.

Roberts, D. A., M. L. Goldstein, L. W. Klein, and W. H. Matthaeus (1987), Origin and evolution of fluctuations in the solar wind: Helios observations and Helios-Voyager comparisons, *J. Geophys. Res.*, *92*, 12,023–12,035, doi:10.1029/JA092iA11p12023.

Ruffolo, D., W. H. Matthaeus, and P. Cuychai (2004), Separation of magnetic field lines in two-component turbulence, *Astrophys. J.*, *614*, 420–434, doi:10.1086/423412.

Smith, C. W., J. L. Heureux, N. F. Ness, M. H. Acuna, L. F. Burlaga, and J. Scheiffele (1998), The ACE magnetic fields experiment, *Space Sci. Rev.*, *86*, 613–632, doi:10.1023/A:1005092216668.

Smith, C. W., W. H. Matthaeus, G. P. Zank, N. F. Ness, S. Oughton, and J. D. Richardson (2001), Heating of the low-latitude solar wind by dissipation of turbulent magnetic fluctuations, *J. Geophys. Res.*, *106*, 8253–8272, doi:10.1029/2000JA000366.

Taylor, G. I. (1938), The spectrum of turbulence, *Proc. R. Soc. A*, *164*, 476–490.

Tu, C. Y., and E. Marsch (1995), MHD structures, waves and turbulence in the solar wind, *Space Sci. Rev.*, *73*, 1–210, doi:10.1007/BF00748891.

Velli, M. (2003), MHD turbulence and the heating of astrophysical plasma, *Plasma Phys. Controlled Fusion*, *45*, A205, doi:10.1088/0741-3335/45/12A/014.

Weygand, J. M., W. H. Matthaeus, S. Dasso, M. G. Kivelson, and R. J. Walker (2007), Taylor scale and effective magnetic Reynolds number determination from the plasma sheet and the solar wind magnetic field fluctuations, *J. Geophys. Res.*, *112*, A10201, doi:10.1029/2007JA012486.

Weygand, J. M., W. H. Matthaeus, S. Dasso, and M. G. Kivelson (2009), Anisotropy of the Taylor scale and the correlation scale in plasma sheet and solar wind magnetic field fluctuations, *J. Geophys. Res.*, *114*, A07213, doi:10.1029/2008JA013766.

Weygand, J. M., W. H. Matthaeus, M. El Alaoui, S. Dasso, and M. G. Kivelson (2010), Anisotropy of the Taylor scale and the correlation scale in plasma sheet magnetic field fluctuations as a function of auroral electrojet activity, *J. Geophys. Res.*, *115*, A12250, doi:10.1029/2010JA015499.

Williams, L. L., G. P. Zank, and W. H. Matthaeus (1995), Dissipation of pickup-induced waves: A solar wind temperature increase in the outer heliosphere?, *J. Geophys. Res.*, *100*, 17,059–17,067, doi:10.1029/95JA01261.

S. Dasso, Instituto de Astronomía y Física del Espacio, Departmento de Física, Facultad de Ciencias Exactas y Naturales, Universidad de Buenos Aires, CC 67 Suc. 28, Buenos Aires City E-1428, Argentina.

M. G. Kivelson, Department of Earth and Space Sciences, University of California, 3845 Slichter Hall, 595 Charles E. Young Dr., PO Box 951567, Los Angeles, CA 90095-1567, USA.

W. H. Matthaeus, Bartol Research Institute, Department of Physics and Astronomy, University of Delaware, Newark, DE 19716, USA.

J. M. Weygand, Institute of Geophysics and Planetary Physics, University of California, 3845 Slichter Hall, 603 Charles E. Young Dr., PO Box 951567, Los Angeles, CA 90095-1567, USA. (jweygand@igpp.ucla.edu)